Relativistic Coulomb wave functions in momentum space

A. H. Sørensen
Institute of Physics and Astronomy, University of Aarhus, DK-8000 Aarhus C, Denmark

A. Belkacem
Lawrence Berkeley Laboratory, 1 Cyclotron Road, Berkeley, California 94720
(Received 16 June 1993)

In this paper, momentum-space wave functions are obtained for unbounded relativistic motion of single electrons in a Coulomb potential. The waves are expressed in terms of a simple contour integral which is easily evaluated numerically. Various examples for motion around a bare uranium nucleus are displayed including negative-energy solutions and dependence on partial-wave angular momentum.

PACS number(s): 03.65.−w, 11.80.Et, 11.10.Qr

I. INTRODUCTION

Momentum-space wave functions for single electrons bound in a Coulomb potential have been provided by many authors both for nonrelativistic and relativistic motion. For the relativistic case we may refer the reader to, e.g., Rubinowicz [1] and Lévy [2]. The situation for unbounded motion in a Coulomb field is — to the best of the knowledge of the present authors — quite different. In this case, solutions in momentum space have been published for nonrelativistic motion only; see the papers [3–10]. Motivated by this apparent deficiency, we report below on a computation of Coulomb wave functions in momentum space for unbounded relativistic motion. The waves obviously appear highly localized. This feature is of substantial advantage in calculations including evaluation of certain matrix elements as discussed, for instance, by Guth and Mullin [10]. The applications we have in mind lie within the realm of relativistic atomic collisions. Examples could be bremsstrahlung and similar processes.

In order to obtain momentum-space wave functions, two different approaches may be followed. One possibility is first to determine the wave functions in configuration space and subsequently perform a Fourier transformation. The second possibility is first to transform the wave equation into an (integral) equation valid in momentum space and then solve this equation directly. For bounded motion, the paper by Rubinowicz [1] relies on the former approach, whereas Lévy [2] applies the latter. In the present paper we shall make use of the availability of configuration-space solutions for the unbounded Coulomb problem and perform a Fourier transformation to obtain the corresponding momentum-space wave functions. We shall give general expressions for the Fourier transforms and describe a way to obtain the momentum waves for unbounded motion numerically. Towards the end, various examples of momentum-space Coulomb waves will be displayed and discussed.

II. GENERAL EXPRESSIONS

As opposed to the nonrelativistic case, the continuum solutions to the Dirac equation for an electron moving in a pure Coulomb potential cannot be given in closed form. It is necessary to expand in partial waves. Expressions for relativistic partial Coulomb waves in configuration space have been given, e.g., by Rose [11], Eichler [12], and Greiner [13].

Let the source of the Coulomb field be a charge Ze and let the total energy of the electron of mass m be $E \equiv Wmc^2$ where $|W| > 1$. The partial waves corresponding to a total angular momentum quantum number j are characterized by the quantum number $\kappa = \pm(j + \frac{1}{2})$, which may take on any nonzero integer value, and by the magnetic quantum number μ, which may assume the values $\mu = -j, -(j-1), ..., j-1, j$. They read

$$\psi(\mathbf{r},t) = \begin{pmatrix} g(r)\Omega_\kappa^\mu(\Theta,\Phi) \\ if(r)\Omega_{-\kappa}^\mu(\Theta,\Phi) \end{pmatrix} \exp(-iWct/\lambda_C) , \quad (1)$$

where the Compton wavelength $\lambda_C = \hbar/mc$ appears as the natural unit of length. The Ω_κ^μ functions are the usual spin-angular functions defined as

$$\Omega_\kappa^\mu = \sum_{m=\pm 1/2} C(l, \tfrac{1}{2}, j; \mu - m, m) Y_l^{\mu-m}(\Theta,\Phi)\chi^m, \quad (2)$$

where the C factor multiplying the spherical harmonic Y_l^m is a Clebsch-Gordan coefficient, cf. [11,14], and $\chi^{\pm 1/2}$ a Pauli spinor. The j quantum number may be reconstructed from κ as $j = |\kappa| - \frac{1}{2}$ while the l quantum number assumes the value

$$l = \begin{cases} \kappa & \text{for } \kappa > 0 \\ -\kappa - 1 & \text{for } \kappa < 0. \end{cases} \quad (3)$$

The expressions for the radial waves are

$$\begin{aligned} g(r) &= N_g (2k_0 r)^{s-1} \operatorname{Re}[e^{i\delta}(s + i\eta)X] , \\ f(r) &= N_f (2k_0 r)^{s-1} \operatorname{Im}[e^{i\delta}(s + i\eta)X] , \end{aligned} \quad (4)$$

where X is defined as

$$X = e^{-ik_0 r} F(s + 1 + i\eta, 2s + 1, i2k_0 r) , \quad (5)$$

F is the degenerate hypergeometric function, and Re[ ] and Im[ ] denote the real and the imaginary part of [ ], respectively. The normalization factors read

$$N_g = 2\left(\frac{k_0}{\pi\lambda_C^2}\right)^{1/2} e^{\pi\eta/2}\frac{|\Gamma(s+i\eta)|}{\Gamma(2s+1)}[S_W(W+1)]^{1/2}\,,$$
$$N_f = -N_g S_W\left(\frac{W-1}{W+1}\right)^{1/2}\,, \tag{6}$$

where $S_W \equiv W/|W|$ is the sign of the energy. Note that the sign of the ratio N_f/N_g changes with that of the energy. The parameters k_0, η, and δ are defined as

$$k_0 = \frac{\sqrt{W^2-1}}{\lambda_C}\,,\quad \eta = \frac{\zeta W}{k_0\lambda_C}\,,\quad e^{2i\delta} = \frac{-\kappa+i\eta/W}{s+i\eta}\,, \tag{7}$$

where ζ and s assume the values

$$\zeta \equiv \alpha Z\,,\qquad s = \sqrt{\kappa^2-\zeta^2} \tag{8}$$

and α denotes the fine-structure constant. Note that k_0 corresponds to the momentum of a free electron of energy Wmc^2. The wave functions are normalized on the energy scale, that is,

$$\int d^3r\ \psi^\dagger_{\tilde{W}}(\mathbf{r})\psi_W(\mathbf{r}) = \delta(W-\tilde{W})\delta_{\tilde{\kappa},\kappa}\delta_{\tilde{\mu},\mu}\,, \tag{9}$$

where the quantum numbers $\tilde{\kappa}$ and $\tilde{\mu}$ belong to the state of energy $\tilde{W}$.

Consider now the Fourier transform of the wave function $\psi(\mathbf{r})$ defined as

$$\psi(\mathbf{k}) = \frac{1}{(2\pi)^{3/2}}\int d^3r\ \psi(\mathbf{r})e^{-i\mathbf{k}\cdot\mathbf{r}}\,. \tag{10}$$

Insertion of the expressions (1) and (2) and subsequent integration over angles transforms Eq. (10) into

$$\psi(\mathbf{k}) = i^{-l}\begin{pmatrix} g(k)\Omega^\mu_\kappa(\Theta_k,\Phi_k) \\ -S_\kappa f(k)\Omega^\mu_{-\kappa}(\Theta_k,\Phi_k)\end{pmatrix}\,, \tag{11}$$

with (Θ_k,Φ_k) denoting the polar and azimuthal angles of $\mathbf{k}$ and $S_\kappa \equiv \kappa/|\kappa|$, cf. [15]. The $g, f(k)$ functions entering (11) read

$$g(k) = (2/\pi)^{1/2}\int_0^\infty dr\ r^2 g(r) j_l(kr)\,,$$
$$f(k) = (2/\pi)^{1/2}\int_0^\infty dr\ r^2 f(r) j_{\bar{l}}(kr)\,, \tag{12}$$

where j_l denotes a spherical Bessel function of order l and

$$\bar{l} = l - S_\kappa. \tag{13}$$

Insertion of the expressions (4) and (5) into (12) yields

$$g(k) = N_g\frac{2^{s-1}}{k_0^3}\sqrt{\frac{2}{\pi}}\ \mathrm{Re}[e^{i\delta}(s+i\eta)\tilde{X}(l,\sigma,s,\eta)]\,,$$
$$f(k) = N_f\frac{2^{s-1}}{k_0^3}\sqrt{\frac{2}{\pi}}\ \mathrm{Im}[e^{i\delta}(s+i\eta)\tilde{X}(\bar{l},\sigma,s,\eta)]\,, \tag{14}$$

where the quantity $\tilde{X}$ is defined as

$$\tilde{X}(l,\sigma,s,\eta) \equiv \int_0^\infty dx\ x^{s+1}j_l(\sigma x)e^{-ix} \times F(s+1+i\eta, 2s+1, 2ix)\,, \tag{15}$$

and $\sigma \equiv k/k_0$. The configuration-space normalization (9) implies a similar normalization in momentum space, that is, $g(k), f(k)$ fulfill the requirement

$$\int_0^\infty dk\ k^2[g_{\tilde{W}}g_W + f_{\tilde{W}}f_W] = \delta(W-\tilde{W})\,, \tag{16}$$

where it is understood that the same value of κ be chosen for the two states of energy W and $\tilde{W}$.

The key quantity to be evaluated to obtain the momentum waves g, f of Eq. (14) obviously is $\tilde{X}$ of Eq. (15). Inspired by the approach used by Rubinowicz [1] for bound states, we express $j_l(z)$ in terms of the spherical Hankel functions $h_l^{(1)}(z)$ and $h_l^{(2)}(z)$, i.e.,

$$\begin{aligned} j_l(z) &= \frac{1}{2}[h_l^{(1)}(z) + h_l^{(2)}(z)] \\ &= \frac{i^{l+1}}{2z}\left((-1)^{l+1}e^{iz}\sum_{k=0}^{l}(l+\tfrac{1}{2},k)(-2iz)^{-k}\right. \\ &\qquad \left. + e^{-iz}\sum_{k=0}^{l}(l+\tfrac{1}{2},k)(2iz)^{-k}\right)\,, \end{aligned} \tag{17}$$

where

$$(l+\tfrac{1}{2},k) = \frac{(l+k)!}{k!\Gamma(l-k+1)}\,, \tag{18}$$

see also [14]. Insertion of Eqs. (17) and (18) into Eq. (15) yields

$$\begin{aligned} \tilde{X}(l,\sigma,s,\eta) = i^l\sum_{k=0}^{l}\frac{(l+k)!}{k!\Gamma(l-k+1)}\left(\frac{i}{2\sigma}\right)^{k+1} \\ \times\left((-1)^{l+1}\int_0^\infty dx\ x^{s-k}e^{i(\sigma-1)x}F\right. \\ \left. +(-1)^k\int_0^\infty dx\ x^{s-k}e^{-i(\sigma+1)x}F\right)\,, \end{aligned} \tag{19}$$

where the arguments of the hypergeometric function are identical to those appearing in Eq. (15), that is, $F = F(s+1+i\eta, 2s+1, 2ix)$.

Below, we aim at a determination of $\tilde{X}$ on the basis of Eq. (19). In Sec. IV we substitute the degenerate hypergeometric series for F and integrate term by term. This standard procedure, however, works only for $k > k_0$ as we shall see. To tract the general case, an integral representation of F is introduced in Sec. V. The sub-

sequent computation of X is performed by means of an interchange of the order of integration.

III. INTERMEZZO: BOUND STATES

Let us digress for a moment and briefly quote a few results valid for bound states: The wave function in configuration space is again decomposed according to the prescription given in Eqs. (1)–(3). The radial waves are products of an exponential, a polynomial, and a factor of r^{s-1} in close analogy to the nonrelativistic case, see, e.g. [11]. For the ground state, whose energy is simply smc^2, the radial waves reduce to

$$g(r) = N_0 \left(\frac{r}{\lambda_C}\right)^{s-1} e^{-\alpha Z r/\lambda_C} ,$$
$$f(r) = -\left(\frac{1-s}{1+s}\right)^{1/2} g(r) , \tag{20}$$

with N_0 defined as

$$N_0 = \frac{(2\alpha Z)^{s+1/2}}{[2\Gamma(2s+1)]^{1/2}} (1+s)^{1/2} \lambda_C^{-3/2} . \tag{21}$$

The g and f functions fulfill the normalization requirement

$$\int_0^\infty dr\, r^2 (g^2 + f^2) = 1 . \tag{22}$$

For the momentum waves, the expressions (10)–(13) still hold. Results for $g(k)$ and $f(k)$ obtained by direct Fourier transformation have been presented in [1]. Direct solution of the Dirac equation in momentum space yields identical answers [2]. The g, f functions are in general expressed by means of a nondegenerate hypergeometric function. For the ground state, however, the radial functions may be written simply as

$$g(k) = N_0^{(k)} \frac{1}{k\lambda_C} \frac{\Gamma(s+1)}{(1+k_Z^2\lambda_C^2)^{(s+1)/2}} \sin[(s+1)\delta] ,$$
$$f(k) = N_0^{(k)} \sqrt{\frac{1-s}{1+s}} \frac{1}{k\lambda_C} \left[\frac{\Gamma(s+1)\cos[(s+1)\delta]}{(1+k_Z^2\lambda_C^2)^{(s+1)/2}} \right.$$
$$\left. - \frac{\Gamma(s)\sin(s\delta)}{k_Z\lambda_C(1+k_Z^2\lambda_C^2)^{s/2}} \right] , \tag{23}$$

with $k_Z \equiv k/\alpha Z = k/\zeta$, $\delta \equiv \arctan(k_Z\lambda_C)$, and $N_0^{(k)}$ defined as

$$N_0^{(k)} = 2^{s+1/2} \left(\frac{1+s}{\alpha Z \pi \Gamma(2s+1)}\right)^{1/2} \lambda_C^{3/2} . \tag{24}$$

The normalization in momentum space follows that in configuration space, i.e., an expression similar to Eq. (22) holds with r replaced by k.

IV. EVALUATION OF $\tilde{X}$ FOR $k > k_0$

Let us turn again to the determination of momentum-space wave functions for unbounded motion. We need to evaluate $\tilde{X}$, Eq. (19). In order to compute the integral, a convergence factor $\exp(-\epsilon x)$ is multiplied on the integrands. The second integral, for instance, then reads

$$\int_0^\infty dx\, x^{s-k} e^{-i(\sigma+1)x} F$$
$$= \lim_{\epsilon\to 0+} \int_0^\infty dx\, x^{s-k} e^{-(i[1+\sigma]+\epsilon)x} F$$
$$\equiv \lim_{\epsilon\to 0+} Y_\epsilon^{(2)} . \tag{25}$$

By insertion of the degenerate hypergeometric series for $F \equiv F(s+1+i\eta, 2s+1, 2ix)$, $Y_\epsilon^{(2)}$ may be expressed as

$$Y_\epsilon^{(2)} = \sum_{n=0}^\infty \frac{(s+1+i\eta)_n (2i)^n}{(2s+1)_n n!}$$
$$\times \int_0^\infty dx\, x^{s+n-k} e^{-(i[1+\sigma]+\epsilon)x} , \tag{26}$$

where the symbol $(a)_n$ has the usual meaning

$$(a)_n = a(a+1)(a+2)\cdots(a+n-1), \qquad (a)_0 = 1. \tag{27}$$

The integral over x is convergent for the values of s, n, and k under consideration and, upon x integration, Eq. (26) transforms into

$$Y_\epsilon^{(2)} = \frac{\Gamma(s+1-k)}{(\epsilon+[1+\sigma]i)^{s+1-k}} \sum_{n=0}^\infty \frac{(s+1+i\eta)_n (s+1-k)_n}{(2s+1)_n n!} \left(\frac{2i}{\epsilon+[1+\sigma]i}\right)^n$$
$$= \frac{\Gamma(s+1-k)}{(\epsilon+[1+\sigma]i)^{s+1-k}} F\left(s+1+i\eta, s+1-k; 2s+1; \frac{2}{1+\sigma-i\epsilon}\right) , \tag{28}$$

cf. [14]. The radius of convergence for the hypergeometric series $F(\cdot,\cdot;\cdot;z)$ is 1, i.e., the series is convergent only for $|z| < 1$. Since it is intended to take the limit $\epsilon \to 0+$, cf. Eq. (25), convergence of (28) is assured only for $\sigma > 1$, i.e., for large momenta, $k > k_0$.

The treatment for the first integral in Eq. (19) is quite similar. By application of the Kummer transformation $F(a,b,z) = \exp(z)F(b-a,b,-z)$ [14], the expression for $Y_\epsilon^{(1)}$ becomes

$$Y_\epsilon^{(1)} = \frac{\Gamma(s+1-k)}{(\epsilon-[1+\sigma]i)^{s+1-k}} \sum_{n=0}^{\infty} \frac{(s-i\eta)_n (s+1-k)_n}{(2s+1)_n n!} \left(\frac{-2i}{\epsilon-[1+\sigma]i}\right)^n$$
$$= \frac{\Gamma(s+1-k)}{(\epsilon-[1+\sigma]i)^{s+1-k}} F\left(s-i\eta, s+1-k; 2s+1; \frac{2}{1+\sigma+i\epsilon}\right) . \tag{29}$$

Again, convergence requires large momenta, i.e., $k > k_0$ in the limit $\epsilon \to 0+$.

Upon substitution of the limiting forms of $Y_\epsilon^{(1,2)}$ for the integrals in Eq. (19), the final expression for $\tilde{X}(l,\sigma,s,\eta)$ is

$$\tilde{X} = \frac{e^{i(l-s)\pi/2}}{(1+\sigma)^{s+2}} \sum_{k=0}^{l} \frac{(l+k)!\Gamma(s+1-k)}{k!\Gamma(l-k+1)} \left(\frac{1+\sigma}{2\sigma}\right)^{k+1} \sum_{n=0}^{\infty} \frac{e^{i(s-l)\pi}(s-i\eta)_n + (s+1+i\eta)_n}{(2s+1)_n n!} (s+1-k)_n \left(\frac{2}{1+\sigma}\right)^n \tag{30}$$

for $k \equiv \sigma k_0 > k_0$.

V. EVALUATION OF $\tilde{X}$ FOR ALL k

In order to obtain $\tilde{X}$ for all values of k, we shall now apply an integral representation of the confluent hypergeometric function and, subsequently, interchange the order of integration. It turns out to be practical to apply a representation in terms of a contour integral, as integrals are to be done numerically and contours may be chosen such as to avoid regions near poles in most cases.

According to [16], the degenerate hypergeometic function may be represented as

$$F(s+1+i\eta, 2s+1, 2ix) = -\frac{\Gamma(2s+1)\Gamma(-s-i\eta)}{2\pi i \Gamma(s-i\eta)} \oint_1^{(0+)} dt\, e^{2ixt}(-t)^{s+i\eta}(1-t)^{s-1-i\eta} . \tag{31}$$

Here, the contour starts at $t=1$, encircles the origin once in the positive sense, and closes at $t=1$, and all powers have their principal values. By inclusion of the usual convergence factor, insertion of the contour-integral representation (31) in the expression (19) for $\tilde{X}(l,\sigma,s,\eta)$ yields

$$\tilde{X} = -\frac{\Gamma(2s+1)\Gamma(-s-i\eta)}{2\pi i\Gamma(s-i\eta)} i^l \sum_{k=0}^{l} \frac{(l+k)!}{k!\Gamma(l-k+1)} \left(\frac{i}{2\sigma}\right)^{k+1}$$
$$\times \lim_{\epsilon\to 0+} \left((-1)^{l+1} \oint_1^{(0+)} dt\, (-t)^{s+i\eta}(1-t)^{s-1-i\eta} \int_0^\infty dx\, x^{s-k} e^{(-\epsilon+i[\sigma-1+2t]x)} \right.$$
$$\left. + (-1)^k \oint_1^{(0+)} dt\, (-t)^{s+i\eta}(1-t)^{s-1-i\eta} \int_0^\infty dx\, x^{s-k} e^{(-\epsilon-i[\sigma+1-2t]x)} \right) . \tag{32}$$

Interchange of the order of integration and subsequent computation of the x integrals further transform this expression into

$$\tilde{X} = -\frac{\Gamma(2s+1)\Gamma(-s-i\eta)}{2\pi i\Gamma(s-i\eta)} i^l \lim_{\epsilon\to 0+} \oint_1^{(0+)} dt\, (-t)^{s+i\eta}(1-t)^{s-1-i\eta} \sum_{k=0}^{l} \frac{(l+k)!\Gamma(s-k+1)}{k!\Gamma(l-k+1)} \left(\frac{i}{2\sigma}\right)^{k+1}$$
$$\times \left[\frac{(-1)^{l+1}}{(\epsilon+i[1-\sigma-2t])^{s+1-k}} + \frac{(-1)^k}{(\epsilon+i[1+\sigma-2t])^{s+1-k}} \right] , \tag{33}$$

where all summations are performed in the integrand since it is intended to perform only a single contour integration for each setting of the parameters in the numerical calculation.

The order of the x and the t integrations may be reversed as above provided

$$-\epsilon - 2\mathrm{Im}t < 0 \tag{34}$$

everywhere on the contour of integration, that is, the contour is not allowed to dive as far as $\epsilon/2$ below the real axis. [If the Kummer transformation were to be applied as in Eq. (29), the sign on Imt would be reversed in (34).] Equation (33) reveals poles at

$$t = \frac{1\mp\sigma}{2} - i\frac{\epsilon}{2} . \tag{35}$$

It is evident that these poles are to be outside the closed contour of integration. In view of the positioning (35), the contour is chosen as sketched in Fig. 1. It consists of two circular arcs and a straight line segment: It starts as a circle centered on the real axis at $1-R$ and with a radius R slightly larger than 0.5, the polar angle extending from 0 up to $\theta_m \equiv \pi + \epsilon/3R$, then continues as a straight line heading straight in the direction of $t = 1$ and finally ends as a circular arc of radius $t_1 \equiv (3+\sigma)/8$ and centered on the real axis at $1 - t_1$, the polar angle decreasing from θ_m to 0. In case $\sigma > 1$, t_1 is chosen to have the value 0.3. It should be noted that although the powers in Eq. (31) are supposed in general to have their principal values, the variation of the argument of $-t$ should be continuous when the real axis is crossed from below between 0 and 1 on the return on the smaller circular arc. As a check of our procedure, the degenerate hypergeometric function $F(s+1+i\eta, 2s+1, 2ix)$ has been computed numerically according to Eq. (31) with the above contour. The integrations are performed simply according to the Simpson rule, cases with $s < 1$ requiring a splitting of the integrals over the arcs near $\theta = 0$. Variation of σ and the radius R shows explicitly independence of the choice of contour. All values of κ and W (which defines s and η) are tractable, as are all values of x. The results for F agree with those obtained by a routine based on a series expansion of the confluent hypergeometric function.

At this point it should be mentioned that contour-integral representations of the confluent hypergeometric function have been applied by a number of authors, in particular Nordsieck [5], Pradhan [6], and Ford [7] (see also Chen and Chen [4]), to obtain momentum waves in the nonrelativistic case. After interchange of the orders of integration and subsequent computation of the Fourier integral, the function to be integrated along the contour in the complex plane is analytic (see remarks in [6] on branch cuts), and the Cauchy integral theorem may be applied. In the relativistic case, however, this does not hold true as is evident from Eq. (33), which displays non-integer negative powers of $t-t_{pole}$ where t_{pole} are the pole values listed in Eq. (35). Consequently, it is necessary to perform the t integration numerically.

In the numerical evaluation of $\tilde{X}$ according to Eq. (33), the convergence parameter ϵ attains a small but finite value, and the outer radius of the integration contour is chosen as $R = 0.500\,01$. The integration is performed by a simple Simpson routine as for F with a splitting of the integration over the circular arcs at $\theta = 0.02$ maintained for $s < 1$. For σ approaching the critical value 1, convergence is assured by splitting the integration over angle despite the value of s. It was found adequate to perform this splitting for values of σ between 0.9 and 1.1 with splitting angles at $\theta_{split} = 0.08 + 2|1-\sigma|$ and $\theta_m - \theta_{split}$ (for $s < 1$ the splitting at the lower angle is maintained at 0.02).

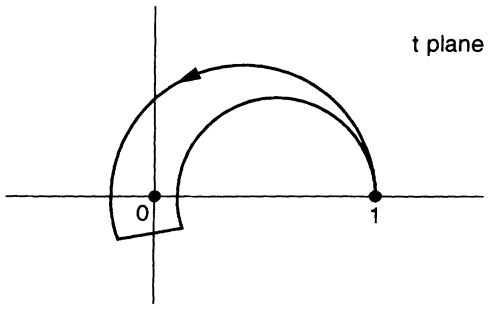

FIG. 1. Contour in complex t plane applied in the integral representation of the confluent hypergeometric function, Eq. (31).

The variation of $\tilde{X}$ with σ is smooth except, as expected, in the region near $\sigma = 1$, where large and rapid variations are encountered. The details of the excursions of $\tilde{X}$ in this region depend on the value of the convergence parameter ϵ. For $\sigma > 1$ and $\epsilon \to 0+$, values obtained by the contour-integral prescription (33) approach those obtained by the summation (30). Indeed, if a finite value of ϵ is introduced also in the latter expression, cf. Eqs. (28) and (29), very good agreement between the results of the two procedures is revealed in the region $\sigma > 1$ for any value of the set ϵ, κ, and W. To be specific, a 251-point Simpson integration for each segment of the contour (the two circular arcs—or fractions thereof when split—being treated simultaneously) leads to a relative deviation of the contour-integral results for the g and f functions of less than 1×10^{-5} from the converged result of the summation (for finite ϵ) for $\sigma - 1 > 0.02$. By increasing the number of steps in the Simpson integration to 1001, the same precision holds true down to $\sigma - 1 \cong 0.002$. It should be stressed that since the two methods for determining $\tilde{X}$ are completely independent, the above precision checks constitute very important checks of the overall procedure for calculating momentum waves.

VI. RESULTS FOR $g(k)$ AND $f(k)$

Insertion of $\tilde{X}(l, \sigma, s, \eta)$ and $\tilde{X}(\bar{l}, \sigma, s, \eta)$ in Eq. (14) yields the final results for $g(k)$ and $f(k)$. In the following we shall present a number of such results with $\tilde{X}$ computed numerically according to Eq. (33) for finite values of ϵ.

Figure 2 reveals a standard example with $Z = 92$, $W = 2$, $\kappa = -3$, and $\epsilon = 1 \times 10^{-3}$. The major features observed are (i) the large excursions for k attaining values very near k_0 and (ii) a substantial weight in the region above k_0 extending up to, roughly, $1.5k_0$. The first feature is a result of the electron being unbound and nearly free. The second derives from the acceleration of the electron near the attracting Coulomb center. As to the sensitivity to the convergence parameter, a decrease of the value of ϵ is found to cause only minor changes in the values of g and f for the region covered by the major part of Fig. 2. Indeed, application of the expression (30) valid for $k > k_0$ and corresponding to $\epsilon = 0$ leads to curves for g and f which are indistinguishable from those plotted for $k > 1.01k_0$ except at the local extremes appearing near $k/k_0 = 1.026$ where an increase in the numerical values of 8% is encountered. For the region covered by the inset, the situation is obviously different. Here a decrease of the convergence parameter by an order of magnitude leads to an enlargement of peak heights by an order of magnitude

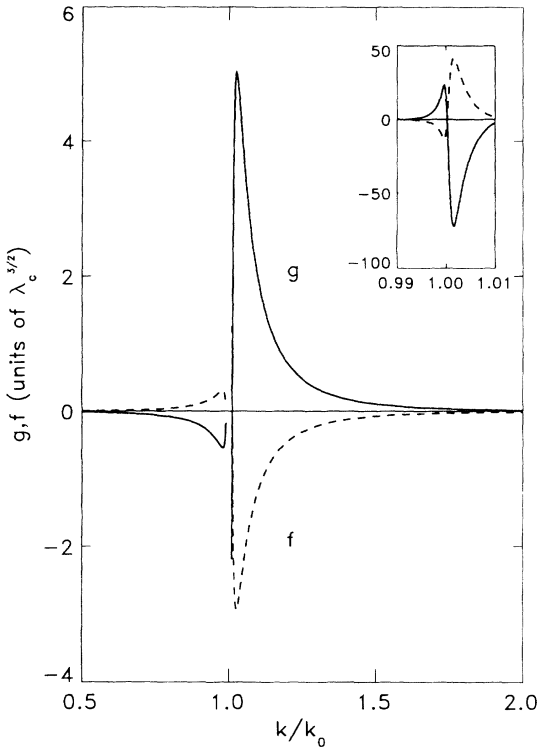

FIG. 2. Functions $g(k)$ and $f(k)$ computed by contour integration for the case of $Z = 92$, $W = 2$, $\kappa = -3$, and $\epsilon = 1 \times 10^{-3}$. The inset shows the details for values of k near k_0, the latter quantity being defined in Eq. (7). The quantity λ_C is the Compton wavelength of the electron, $\lambda_C = \hbar/mc$.

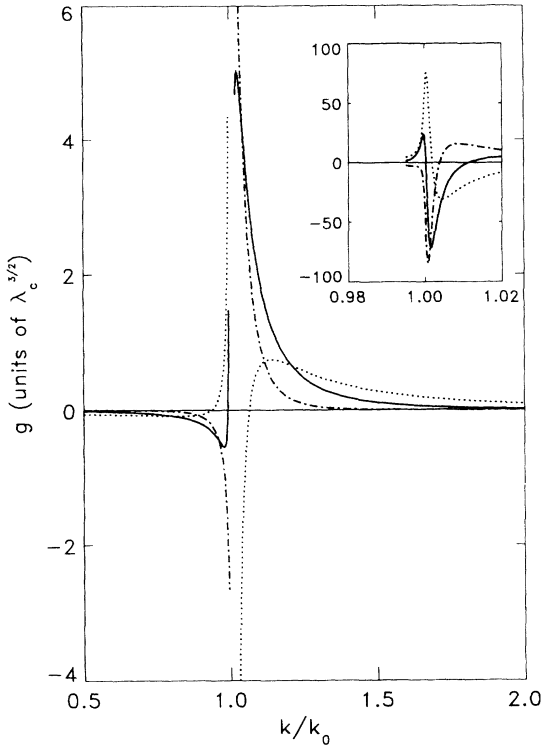

FIG. 3. Function $g(k)$ computed by contour integration for $Z = 92$, $W = 2$, $\epsilon = 1 \times 10^{-3}$, and different values of κ. The solid line corresponds to $\kappa = -3$ (identical to solid curve of Fig. 2), the dotted line is for $\kappa = -1$, whereas the dot-and-dashed line is for $\kappa = -9$. The main plot displays the g function outside the interval [0.995;1.020]; the variation for values of k near k_0 is shown in the inset.

with simultaneous shift of peak positions towards 1.

Figure 3 shows the dependence on κ for fixed values of Z, W, and ϵ (chosen as 92, 2, and 1×10^{-3}). The obvious feature to be observed is the decrease in the region above k_0 with substantial support for increasing value of $|\kappa|$. This is a result of less acceleration in the effective potential for the radial motion due to the angular momentum barrier.

Figure 4 displays the situation for a state of negative energy, namely, $W = -2$ (Z, κ, and ϵ being chosen as in Fig. 2, that is, as 92, -3, and 1×10^{-3}). Repulsion causes the support outside the immediate neighborhood of k_0 to be mainly at values of k smaller than k_0 as opposed to the positive-energy case, cf. Fig. 2.

The bound-state wave functions are obviously quite different from the unbound waves displayed above. As an example, Fig. 5 shows the ground state waves (23) and the corresponding density $k^2(g^2 + f^2)$ for a hydrogen-like uranium ion ($Z = 92$). The g and f functions are smooth and, for the ground state, without any nodes. The density attains its maximum at $k = 0.448\lambda_C^{-1}$ [which value, if converted according to Eq. (7), corresponds to an energy of $W = 1.096$ for a free particle]. At large k values, the functions fall off relatively slowly. Asymptotically, the waves (23) are proportional to the power $k^{-(s+2)}$ and, correspondingly, the density displayed in Fig. 5 falls off as $k^{-2(s+1)}$ which in the present case is, roughly, $k^{-3.48}$.

In order to check orthonormality for our momentum

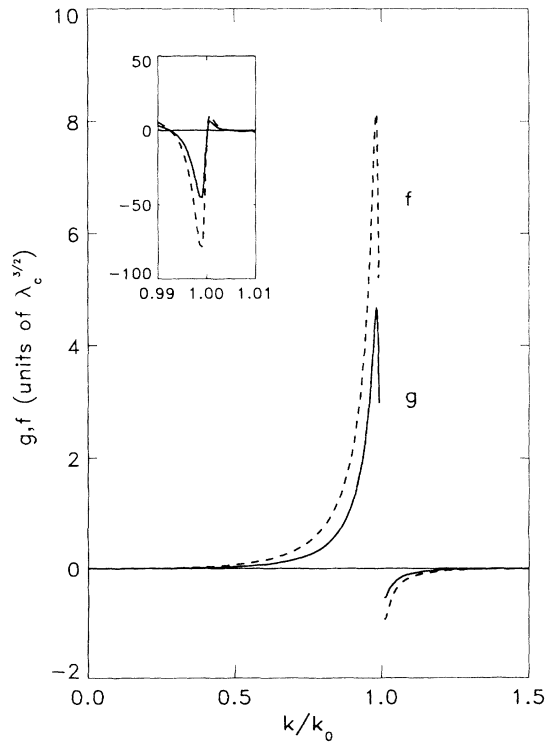

FIG. 4. As in Fig. 2 but with a negative energy of $W = -2$.

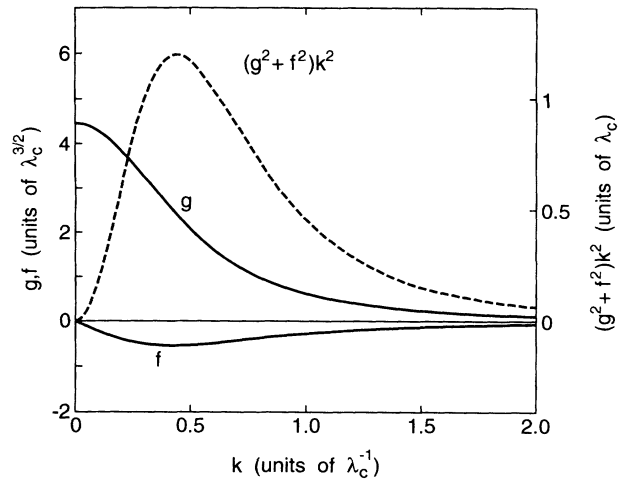

FIG. 5. Momentum waves $g(k)$ and $f(k)$ and the corresponding density $k^2(g^2+f^2)$ for a hydrogenlike uranium ion ($Z=92$), cf. Eq. (23).

waves, the overlap integral defined by the left-hand side of Eq. (16) has been computed in a number of cases. In the limit $\epsilon \to 0+$, the delta function $\delta(W-\tilde{W})$ should result. Figure 6 reveals examples of the overlap as a function of $\tilde{W}$ for three different values of ϵ and W fixed to 2, the remaining parameters being Z=92 and $\kappa=-3$. For

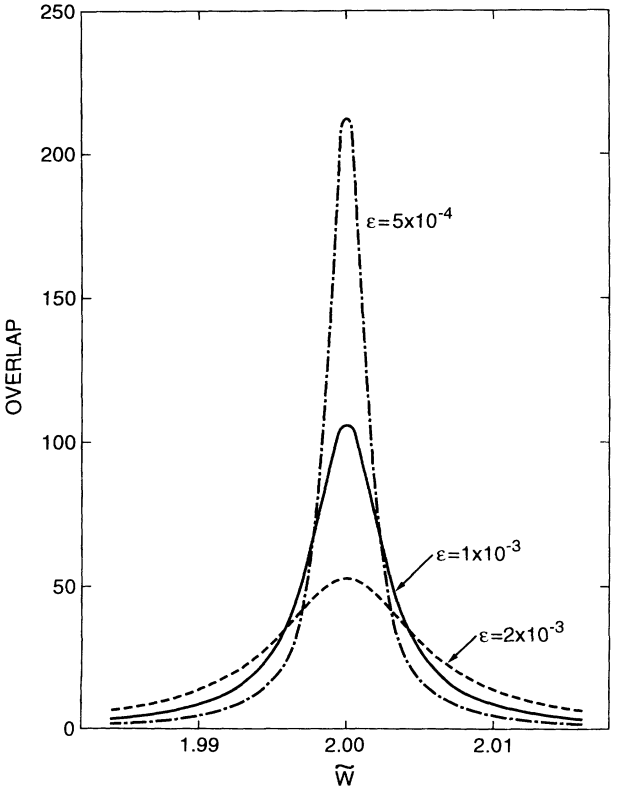

FIG. 6. Overlap integral defined by the left-hand side of Eq. (16) as a function of $\tilde{W}$ for $W=2$, Z=92, $\kappa=-3$, and three different values of ϵ.

$\epsilon = 1\times10^{-3}$, integration of the overlap over the intervals [1.98; 2.02] and [1.95; 2.05] yields 0.904 and 0.960, respectively. Overlap curves similar to those presented in Fig. 6 have been produced for a variety of cases corresponding to different values of ϵ, κ, and W. In all cases, the curves were very close to normalized Lorentzians,

$$Y_L(\Delta W) = \frac{2/\pi\Gamma}{1+(2\Delta W/\Gamma)^2} \,. \tag{36}$$

For the full-drawn curve in Fig. 6 and the interval [1.98;2.02], the rms deviation of Y/Y_L from 1 where Y_L is a normalized Lorentzian of half-width $\Gamma/2 = 2.990\times10^{-3}$ is as low as 0.2%. The half-width turns out to scale linearly with ϵ, which clearly emphasizes the role played by this quantity as a convergence parameter. On the other hand, Γ is independent of κ and the dependence of Γ/k_0 on W is moderate. The results may be summarized as

$$\Gamma/2 \;=\; \epsilon\,\sqrt{W^2-1}\,\mathcal{F}(|W|)\,, \tag{37}$$

where $\mathcal{F}$ is an increasing function of $|W|$ which attains the value 0.831 at W=1.1 and approaches the value 2 asymptotically as W tends towards large values. We have further considered states which are quite far apart in the energy spectrum by computing the overlap of a positive- and a negative-energy state as well as the overlap of unbound states with the ground state specified in Sec. III. In all cases the overlaps were low, although larger than suggested by the tails of the Lorentzians (36). For instance, the overlap of unbound states with $|W|=2$, $\epsilon = 1\times10^{-3}$, and $\kappa=-1$ with the ground state attains values of 3.67×10^{-3} and 1.31×10^{-3} for the positive- and the negative-energy states, respectively. These values are roughly an order of magnitude higher than those predicted by Eq. (36)—but of course still five orders of magnitude smaller than the maximum $Y_L(0)$.

As an additional check of normalization, as another indicator of accuracy, and as yet an illustration of the role played by ϵ as a convergence parameter we have checked norm squares of wave packets which by construction are supposed to be normalized. The waves are packets of partial waves corresponding to a given set of values κ, μ. They are constructed according to the prescription

$$\psi(\mathbf{k}) = \int_{W_a}^{W_b} dW\; C_W \psi_W(\mathbf{k})\,, \tag{38}$$

where ψ_W is a wave of the form (11) of energy W and $1 < W_a < W_b$. Note that while superpositions of this form in configuration space create localized objects out of nonlocalized energy eigenstates, the situation in momentum space is somewhat reversed; starting from the well localized $\psi_W(\mathbf{k})$ superposition produces a broadening. In order that the packets (38) be normalized it is required that the weight factor C_W fulfill the condition

$$1 = \int_{W_a}^{W_b} dW\; |C_W|^2 \tag{39}$$

in view of Eq. (16). We chose the bell-shaped weight $C_W = \sqrt{218\,790}(W_b-W_a)^{-17/2}(W-W_a)^4(W-W_b)^4$,

constructed smooth packets according to Eq. (38) with our spiky g and f functions as input, and computed norm squares. At this point it is important to realize that the latter will not in general come out as a plain 1 due to the finite value of ϵ. There are two reasons. First, the tails of overlaps outside the interval $[W_a; W_b]$, cf. Eq. (36) and discussion above, lead to too low numbers; the deficiency may be estimated roughly as $2\Gamma/\pi(W_b - W_a)$. Second, the variation of C_W on the scale Γ leads to a correction which in the present case is negative and which may be estimated roughly as $[2\Gamma/(W_b - W_a)]^2$. For corrections to be small, $\Gamma/(W_b - W_a)$ obviously needs to be small, that is, ϵ divided by the relative width of the packet needs to be small. Wave packets were created for $Z = 92$ and $\kappa = -1$ with $W_a = 2$ and $W_b = 2.1$. For $\epsilon = 1 \times 10^{-3}$, the norm square was calculated to 0.899. By decreasing ϵ to 1×10^{-4}, the value improved to 0.990, and a further decrease to $\epsilon = 5 \times 10^{-5}$ gave 0.995. In total, it is seen that the deviation from 1 essentially is proportional to ϵ, that is, the normalization integral converges to 1 as ϵ tends to 0. We remind the reader at this point that for given ϵ the precision with which we compute the momentum waves is considerably higher than the three digits given in the last few lines might seem to indicate, cf. final paragraph of Sec. V.

VII. CONCLUDING REMARKS

We have succeeded in determining the wave functions in momentum space for relativistic single electrons in unbound motion in a Coulomb field. Guidelines for practical calculation have been given and examples obtained by simple numerical integration have been displayed. It is our hope that the results may find applications in the future, e.g., in collision problems.

ACKNOWLEDGMENTS

This work was supported by the Danish Natural Science Research Council, and by the Director, Office of Energy Research, Office of Basic Energy Sciences, Chemical Sciences Division, of the U.S. Department of Energy (DOE) under Contract No. DE-AC-03-76SF00098.

[1] A. Rubinowicz, Phys. Rev. **73**, 1330 (1948).
[2] M. Lévy, Proc. R. Soc. London, Ser. **A 204**, 145 (1951).
[3] H. van Haeringen, *Charged-Particle Interactions; Theory and Formulas* (Coulomb Press, Leyden, 1985).
[4] J. C. Y. Chen and A. C. Chen, Adv. At. Mol. Phys. **8**, 71 (1972).
[5] A. Nordsieck, Phys. Rev. **93**, 785 (1954).
[6] T. Pradhan, Phys. Rev. **105**, 1250 (1957).
[7] W. F. Ford, Phys. Rev. **133**, B1616 (1964).
[8] J. Townsend, G. Feldman, and T. Fulton, J. Math. Phys. **13**, 1865 (1972).
[9] J. Schwinger, J. Math. Phys. **5**, 1606 (1964).
[10] E. Guth and C. J. Mullin, Phys. Rev. **83**, 667 (1951).
[11] M. E. Rose, *Relativistic Electron Theory* (Wiley, New York, 1961).
[12] J. Eichler, Phys. Rep. **193**, 165 (1990).
[13] W. Greiner, *Relativistic Quantum Mechanics–Wave Equations* (Springer, Berlin, 1990).
[14] *Handbook of Mathematical Functions,* edited by M. Abramowitz and I. A. Stegun (Dover, New York, 1972).
[15] H.-J. Bär and G. Soff, Physica C **128**, 225 (1985).
[16] *Higher Transcendental Functions*, edited by A. Erdélyi *et al.* (McGraw-Hill, New York, 1953), Vol. I.